引用格式：LIANG Dongbao, ZHANG Rui, SHEN Yufang, et al. Synthesis and Luminescent Properties of $BaLaGa_3O_7:Bi^{3+}$ Phosphors[J]. Acta Photonica Sinica, 2022, 51(3):0316002
梁冬宝,张瑞,申玉芳,等. $BaLaGa_3O_7:Bi^{3+}$荧光粉的制备及发光性能研究[J].光子学报,2022,51(3):0316002

$BaLaGa_3O_7:Bi^{3+}$荧光粉的制备及发光性能研究

梁冬宝,张瑞,申玉芳,张建
(桂林理工大学 材料科学与工程学院 广西光电材料与器件重点实验室 有色金属及材料加工新技术教育部重点实验室,广西 桂林 541004)

摘　要：采用高温固相法合成了$BaLa_{1-x}Ga_3O_7:xBi^{3+}$($0.01\leqslant x\leqslant 0.13$)系列荧光粉。X射线衍射数据和Rietveld精修结果表明,$BaLa_{1-x}Ga_3O_7:xBi^{3+}$荧光粉具有黄长石结构。扫描电镜图像显示,荧光粉的颗粒为不规则形状,尺寸在5～30 μm之间。漫反射光谱表明,$BaLaGa_3O_7$基体对于Bi^{3+}离子掺杂发光具有合适的光学带隙。在348 nm紫外光激发下,$BaLa_{1-x}Ga_3O_7:xBi^{3+}$荧光粉呈现出中心波长位于475 nm的宽带发射。随着Bi^{3+}离子掺杂浓度增加,荧光粉的发射强度出现先增加后减少的趋势,该浓度猝灭发光现象源于偶极-偶极相互作用。其中,$BaLa_{0.89}Ga_3O_7:0.11Bi^{3+}$荧光粉的发射强度达到最大,量子产率为19.2%,且在150℃时的发射强度仍能保持25℃时的69.2%,说明$BaLa_{1-x}Ga_3O_7:xBi^{3+}$荧光粉在近紫外激发白光LED领域具有潜在的应用价值。

关键词：Bi^{3+}离子;镓酸盐;荧光粉;发光性能;白光LED
中图分类号：O482.31　　**文献标识码**：A　　**doi**：10.3788/gzxb20225103.0316002

0　引言

当前,白光发光二极管(Light-Emitting Diode, LED)在照明、显示等领域发挥着不可估量的作用。由于封装工艺简单、经济成本较低等特点,蓝光LED芯片与黄色、红色荧光粉组合成为工业界主流的封装技术[1]。为了满足高显色性的照明需求,紫外LED芯片与三基色荧光粉的组合也是一种较佳的选择。目前,能够被紫外LED芯片激发的商业荧光粉大多数以稀土离子(Ce^{3+}、Tb^{3+}、Eu^{3+}等)作为激活剂[2-4]。由于稀土离子具有丰富的能级结构,蓝色荧光粉的发射光谱会与绿色、红色荧光粉的激发光谱部分重叠,从而造成严重的重吸收,导致白光LED器件在工作时出现发光效率较低和发射颜色失真的现象。如何避免光谱重吸收,已成为当前提高照明效率和品质的重要研究方向。

三价铋离子(Bi^{3+})是一种典型的非稀土离子激活剂,仅对紫外光有较强的吸收能力,可有效避免因光谱重吸收而影响器件发光性能的问题。Bi^{3+}的电子构型为$[Xe]4f^{14}5d^{10}6s^2$,其裸露在外的6s和6p电子对配位环境(如晶体场强、配位数、占位对称性等)非常敏感。当Bi^{3+}离子掺杂到不同类型的基质(如硼酸盐、硅酸盐、锗酸盐、钨酸盐等)时,可以实现从紫外到红色不同颜色的发光[5]。例如,$Cs_3Zn_6B_9O_{21}:Bi^{3+}$蓝色荧光粉[6]、$NaGd_9(SiO_4)_6O_2$蓝色荧光粉[7]、$Ca_3Lu_2Ge_3O_{12}:Bi^{3+}$青色荧光粉[8]、$Ba_2Ga_2GeO_7:Bi^{3+}$青色荧光粉[9]、$Ca_2MgWO_6:Bi^{3+}$黄色荧光粉[10]。此外,通过阳离子取代调控配位环境,在$BaSrGa_4O_8:Bi^{3+}$荧光粉中实现了从橙黄色到绿色的发光颜色调整[11]。目前,就LED照明和显示需求而言,开发一种能被近紫外LED芯片激发的Bi^{3+}掺杂新型荧光粉引起了人们的兴趣。

$BaLaGa_3O_7$是黄长石结构ABC_3O_7(A=Ca, Sr, Ba; B=镧系元素; C=Al, Ga)中的一员。迄今为止,

基金项目：国家自然科学基金(No.52062008),广西自然科学基金(No.2018GXNSFAA050021)
第一作者：梁冬宝(1995—),男,硕士研究生,主要研究方向为无机发光材料。Email: Lbigwatermelon@126.com
导师(通讯作者)：张瑞(1986—),男,副教授,博士,主要研究方向为无机发光材料。Email: rzhang@glut.edu.cn
申玉芳(1977—),女,副教授,博士,主要研究方向为无机发光材料。Email: yuffangshen@gmail.com
收稿日期：2021-08-24;**录用日期**：2021-09-22

以稀土离子为激活剂的$BaLaGa_3O_7$荧光粉相继报道，如$BaLaGa_3O_7:Tm^{3+}$，Dy^{3+}[12]，$BaLaGa_3O_7:Pr^{3+}$，Tb^{3+}[13]荧光粉。然而，以Bi^{3+}离子为激活剂的$BaLaGa_3O_7$荧光粉尚未见研究。本文选择具有良好稳定性的$BaLaGa_3O_7$作为基质材料，采用高温固相法合成了$BaLa_{1-x}Ga_3O_7:xBi^{3+}$荧光粉，通过相关表征手段对其晶体结构、微观形貌和发光性能进行了研究。

1 实验

1.1 样品制备

采用高温固相法合成了$BaLa_{1-x}Ga_3O_7:xBi^{3+}$($0.01\leqslant x\leqslant 0.13$)系列荧光粉。根据化学计量比称取$BaCO_3$(99.99%)、$La_2O_3$(99.99%)、$Ga_2O_3$(99.99%)、$Bi_2O_3$(99.99%)等原料，置于玛瑙研钵中，加入适量无水乙醇后研磨30 min，使其混合均匀。将混合物置于氧化铝坩埚中，在1 100 ℃马弗炉中预烧12小时。冷却至室温后，将前驱体研磨成粉，置于氧化铝坩埚中，在1 300 ℃马弗炉中煅烧8 h。将冷却至室温后的样品研磨成粉末以进行表征。

1.2 样品表征

使用PANalytical Empyrean型X射线衍射仪对样品的晶体结构进行X射线衍射(X-ray diffraction，XRD)测量，测量条件为Cu Kα1辐射($\lambda=1.540\ 59$ Å，1 Å=0.1 nm)，管电压为40 kV，电流为40 mA。使用晶体结构分析软件(General Structure Analysis System，GSAS)对XRD图谱进行Rietveld精修，分析样品的晶体结构参数。使用配备能量色散X射线能谱(Energy Dispersive X-ray Spectroscopy，EDS)的扫描电子显微镜(Scanning Electron Microscope，SEM)测量样品的形貌和元素分布。使用UV3600型紫外-可见-近红外分光光度计记录样品的漫反射光谱(Diffuse Reflectance Spectra，DRS)。使用QuantaMaster 8000型荧光光谱仪记录样品的激发光谱(Photoluminescence Excitation，PLE)、发射光谱(Photoluminescence，PL)和荧光衰减曲线，通过积分球测试粉末样品的量子产率。此外，通过上述光谱仪与THMS 600型精确温度控制的加热制冷台配合测试样品的变温光谱。

2 结果与讨论

2.1 结构与形貌分析

图1(a)为$BaLa_{1-x}Ga_3O_7:xBi^{3+}$($0.01\leqslant x\leqslant 0.13$)样品的XRD图谱。所有样品的衍射峰均与$BaLaGa_3O_7$标准卡片(No.50-1800)吻合，未观察到其他杂质峰的存在，说明合成的样品均为纯相，Bi^{3+}离子的引入并未破坏$BaLaGa_3O_7$基体的晶体结构。通常而言，掺杂离子与晶格离子之间的半径百分比不超过30%时，掺杂离子能够置换晶格离子；半径百分比越小，越容易产生置换。半径百分比计算公式为[14]

$$D_r=\left|\frac{R_m(\mathrm{CN})-R_d(\mathrm{CN})}{R_m(\mathrm{CN})}\right| \tag{1}$$

式中，D_r代表半径百分比，R_m(CN)代表基质晶体中离子半径，R_d(CN)代表掺杂离子半径。在$BaLaGa_3O_7$晶体中，存在Ba^{2+}、La^{3+}和Ga^{3+}三种阳离子，离子半径分别为1.42 Å(CN=8)，1.18 Å(CN=8)和0.47 Å(CN=4)，

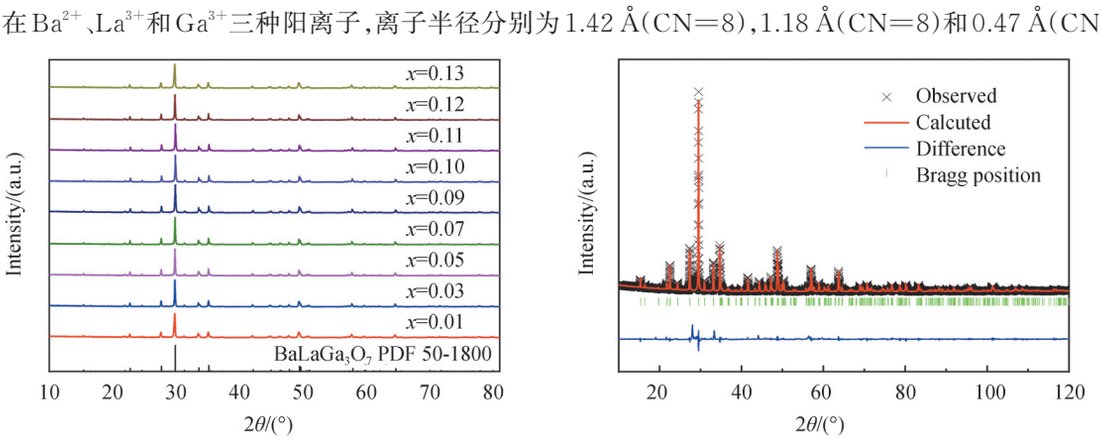

(a) XRD patterns　　(b) Rietveld refinement of $BaLa_{0.89}Ga_3O_7:0.11Bi^{3+}$

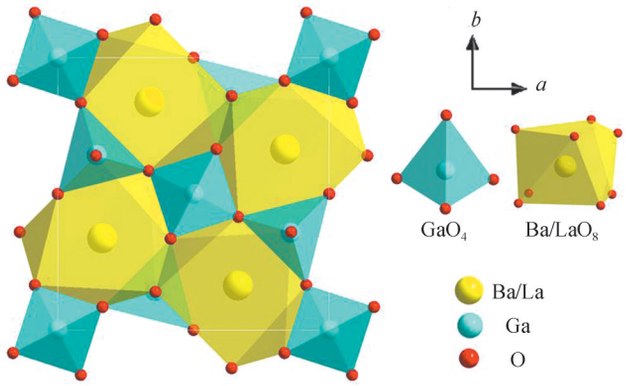

(c) Schematic of crystal structure of $BaLaGa_3O_7$

图1　$BaLa_{1-x}Ga_3O_7:xBi^{3+}$（$0.01\leqslant x\leqslant 0.13$）样品的XRD图谱和$BaLaGa_3O_7$的晶体结构示意图

Fig.1　XRD patterns of $BaLa_{1-x}Ga_3O_7:xBi^{3+}$ ($0.01\leqslant x\leqslant 0.13$) samples and schematic of crystal structure of $BaLaGa_3O_7$

而Bi^{3+}离子的半径为1.11 Å（CN=8）。经计算，La^{3+}离子的D_r值（5%）远小于Ba^{2+}离子的D_r值（21%），根据离子半径相近易于取代的原则，确定Bi^{3+}离子取代La^{3+}离子的晶格位置。为了准确获取样品的晶体结构信息，对$BaLa_{0.89}Ga_3O_7:0.11Bi^{3+}$样品的XRD图谱进行Rietveld精修。如图1(b)所示，样品的衍射峰与精修结果非常吻合。表1展示了Rietveld精修的主要晶体结构参数，其中$R_{wp}=5.49\%$，$R_p=6.18\%$，$\chi^2=7.37$，说明精修结果较为准确，进一步证实了$BaLa_{0.89}Ga_3O_7:0.11Bi^{3+}$样品的黄长石结构。图1(c)为$BaLaGa_3O_7$的晶体结构示意图，晶胞由沿c四方轴的多面体层交替形成，其中四面体位点被Ga^{3+}离子占据，Ba^{2+}和La^{3+}离子以1∶1的比例随机占据十二面体位点。

表1　$BaLa_{0.89}Ga_3O_7:0.11Bi^{3+}$样品Rietveld精修的主要参数

Table 1　Main parameters of Rietveld refinement of the $BaLa_{0.89}Ga_3O_7:0.11Bi^{3+}$ sample

Formula	$BaLa_{0.89}Ga_3O_7:0.11Bi^{3+}$
Space group	P−421m
$a=b$/Å	8.165 6(6)
c/Å	5.402 4(1)
V/Å^3	360.219 4(8)
Z	2
R_{wp}/%	5.49
R_p/%	6.18
χ^2	7.37

图2为$BaLa_{0.89}Ga_3O_7:0.11Bi^{3+}$样品的SEM图像。样品颗粒呈现出不规则的形状，尺寸在5～30 μm之

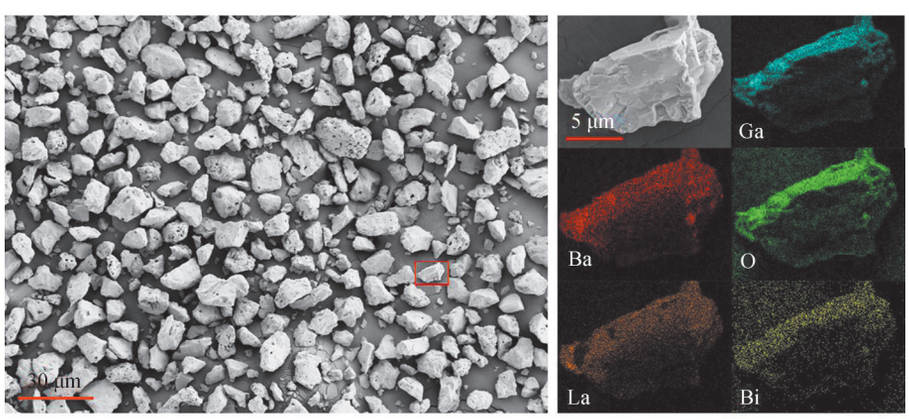

图2　$BaLa_{0.89}Ga_3O_7:0.11Bi^{3+}$样品的SEM图像和EDS元素分布

Fig.2　SEM image and corresponding elemental mappings of $BaLa_{0.89}Ga_3O_7:0.11Bi^{3+}$ sample

间。另外，图中展示了单个颗粒的EDS图像，进一步证实了$BaLa_{0.89}Ga_3O_7:0.11Bi^{3+}$样品由Ba、La、Ga、O和Bi元素组成，各元素在样品中均匀分布，未观察到元素团聚和相分离的现象。

2.2 光学性能分析

图3(a)为$BaLaGa_3O_7$和$BaLa_{0.89}Ga_3O_7:0.11Bi^{3+}$样品的漫反射光谱。可以看出，未掺杂样品的吸收截止边缘位于240 nm左右，源于$BaLaGa_3O_7$基体的本征吸收。当Bi^{3+}离子掺入$BaLaGa_3O_7$基体后，样品在270 nm和350 nm处各有一个吸收峰，这分别归因于Bi^{3+}离子的$^1S_0\rightarrow{}^1P_1$和$^1S_0\rightarrow{}^3P_1$跃迁。此外，$BaLaGa_3O_7$基体的光学带隙E_g可根据Kubelka-Munk吸收函数计算[15]

$$\alpha=(1-R)^2/2R \tag{2}$$

$$(\alpha h\nu)^2=A(h\nu-E_g) \tag{3}$$

式中，α代表吸收率，R代表漫反射率，$h\nu$代表光子能量，A代表比例常数。如图3(b)所示，通过外推$[\alpha h\nu]^2$ vs. $h\nu$曲线的线性部分可知$BaLaGa_3O_7$基质的E_g值为5.12 eV。对于Bi^{3+}离子发光而言，$BaLaGa_3O_7$基体具有合适的光学带隙。

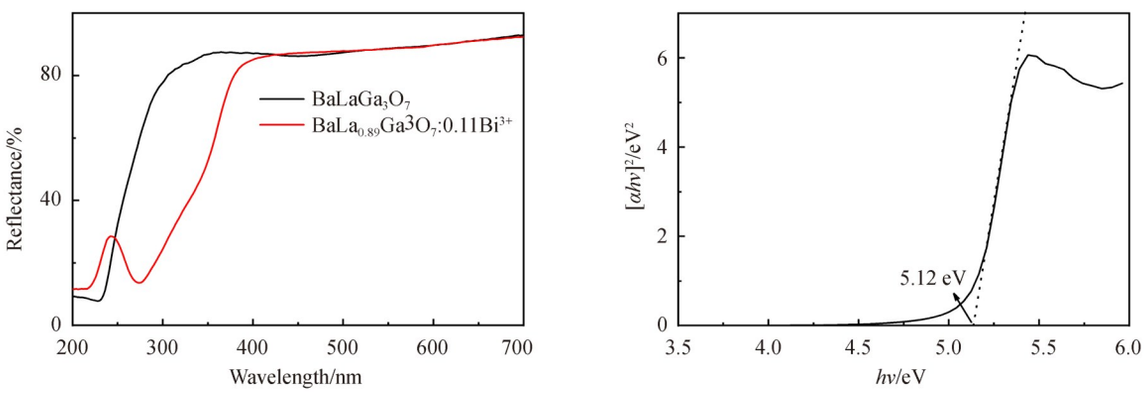

(a) Diffuse reflectance spectra　　(b) Plot of $[\alpha h\nu]^2$ vs. $h\nu$

图3 $BaLaGa_3O_7$基质和$BaLa_{0.89}Ga_3O_7:0.11Bi^{3+}$样品的漫反射光谱

Fig.3 Diffuse reflectance spectra of $BaLaGa_3O_7$ host and $BaLa_{0.89}Ga_3O_7:0.11Bi^{3+}$ sample

图4(a)为$BaLa_{1-x}Ga_3O_7:xBi^{3+}$($0.01\leqslant x\leqslant 0.13$)样品的激发光谱和发射光谱。可以看出，$BaLa_{1-x}Ga_3O_7:xBi^{3+}$样品具有一个归因于$Bi^{3+}$：$^1S_0\rightarrow{}^3P_1$跃迁的宽激发带，峰值位于350 nm左右，与近紫外LED芯片能够较好地匹配。此外，随着掺杂离子浓度的增加，$BaLa_{1-x}Ga_3O_7:xBi^{3+}$样品激发带的峰值位置发生了微小红移，即从340 nm红移到350 nm处。这是因为较大的Bi^{3+}离子取代La^{3+}离子后，会降低该晶格位点周围的晶体场强度，引起晶体场劈裂导致最低的激发能级下降，从而引起激发带的峰值位置红移[16]。在348 nm紫外光激发下，$BaLa_{1-x}Ga_3O_7:xBi^{3+}$样品呈现覆盖375～650 nm波长的宽带发射带，峰值位于475 nm，归因于Bi^{3+}：$^3P_1$

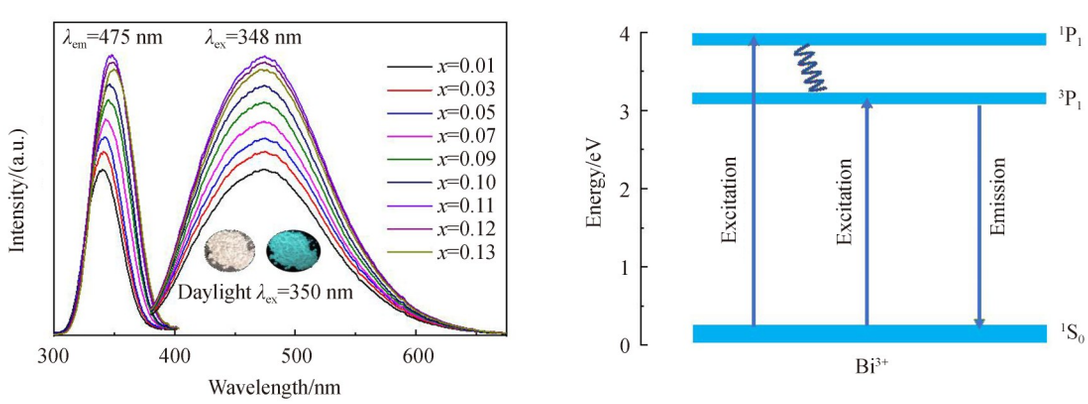

(a) PLE and PL spectra　　(b) Schematic energy level diagram of Bi^{3+} ions

图4 $BaLa_{1-x}Ga_3O_7:xBi^{3+}$($0.01\leqslant x\leqslant 0.13$)样品的荧光光谱和$Bi^{3+}$离子的能级示意图

Fig.4 Fluorescence spectra of $BaLa_{1-x}Ga_3O_7:xBi^{3+}$ ($0.01\leqslant x\leqslant 0.13$) samples and schematic energy level diagram of Bi^{3+} ions

→$^1S_0$跃迁。图4(b)展示了Bi^{3+}离子发光的能级示意图。当被紫外光激发时，位于基态$^1S_0$能级的电子一部分跃迁到$^1P_1$能级，另一部分跃迁到$^3P_1$能级，其中$^1P_1$能级的大部分电子会通过自旋-晶格弛豫跃迁到$^3P_1$能级，因此样品的青光发射来自位于$^3P_1$能级的电子返回到基态。

随着Bi^{3+}离子的含量增加，样品的发射强度逐渐增强，当掺杂含量为0.11时达到最大值，之后发射强度逐渐减弱。这种发光现象归因于浓度猝灭效应。为了究其原因，引入掺杂离子之间能量的临界距离R_c，公式为[17]

$$R_c = 2 \times \left(\frac{3V}{4\pi X_c N} \right)^{1/3} \tag{4}$$

式中，X_c代表最佳掺杂浓度，N代表单位晶胞中La^{3+}离子的数量，V代表单位晶胞的体积。对于$BaLaGa_3O_7:Bi^{3+}$，$X_c=0.11$，$N=2$，$V=357.05$ Å^3。经计算，R_c值约为14.58 Å，远远大于交换相互作用距离(~5 Å)。因此，Bi^{3+}离子之间的浓度猝灭效应不太可能是由交换相互作用引起的，所以可推测电多极相互作用在浓度猝灭现象中起主要作用。电多极相互作用有三种类型，即偶极-偶极相互作用、偶极-四极相互作用和四极-四极相互作用。根据Dexter理论，通过以下式(5)分析电多极相互作用的类型[18]。

$$\log(I/x) = A - (\theta/3)\log x \tag{5}$$

式中，I代表发射强度，x代表掺杂浓度，A代表基质在相同激发条件下的常数，θ代表电多极特性($\theta=6$、8和10分别对应于偶极-偶极、偶极-四极和四极-四极相互作用)。如图5所示，通过对$\log(I/x)$和$\log(x)$的关系进行线性拟合，得到直线的斜率($-\theta/3$)为−1.66，$\theta=4.98$，接近于数值6，表明$BaLa_{1-x}Ga_3O_7:xBi^{3+}$样品的浓度猝灭机理是偶极-偶极相互作用。

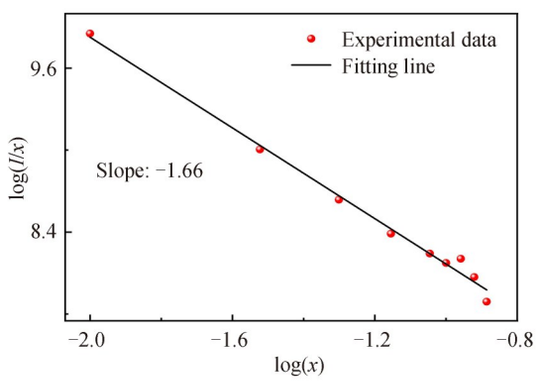

图5 $BaLa_{1-x}Ga_3O_7:xBi^{3+}$($0.01\leqslant x\leqslant 0.13$)样品中$\log(I/x)$与$\log(x)$的关系

Fig5 Relationship between $\log(I/x)$ and $\log(x)$ for $BaLa_{1-x}Ga_3O_7:xBi^{3+}$ ($0.01\leqslant x\leqslant 0.13$) samples

为了更进一步确定Bi^{3+}离子对样品发光的影响，在激发波长348 nm、发射波长475 nm下测试$BaLa_{1-x}Ga_3O_7:xBi^{3+}$($0.01\leqslant x\leqslant 0.13$)样品的荧光衰减曲线，以及对$Bi^{3+}$的荧光寿命进行分析。如图6(a)所示，样品的衰减曲线可通过双指数函数进行很好地拟合[19]。

$$I(t) = A_1 \exp^{-t/\tau_1} + A_2 \exp^{-t/\tau_2} \tag{6}$$

式中，$I(t)$代表在时间为t时的发射强度，A_1和A_2代表该条件下的拟合常数，τ_1和τ_2代表寿命的指数成分。因此，荧光寿命τ计算公式为[20]

$$\tau = \frac{A_1\tau_1^{\ 2} + A_2\tau_2^{\ 2}}{A_1\tau_1 + A_2\tau_2} \tag{7}$$

根据图6(b)的计算结果分析可知，随着Bi^{3+}离子浓度增加，$BaLa_{1-x}Ga_3O_7:xBi^{3+}$样品的荧光寿命逐渐减小。此种变化趋势说明掺杂离子$Bi^{3+}$之间存在着能量转移，非辐射跃迁因掺杂离子浓度增加而逐渐变强，最终引起样品的荧光寿命减小。

量子产率(Quantum Yield，QY)是评估荧光粉性能优劣的关键光学性能之一。选择以发光强度最强的$BaLa_{0.89}Ga_3O_7:0.11Bi^{3+}$样品为代表，对它的量子产率进行测量，计算公式为[10]

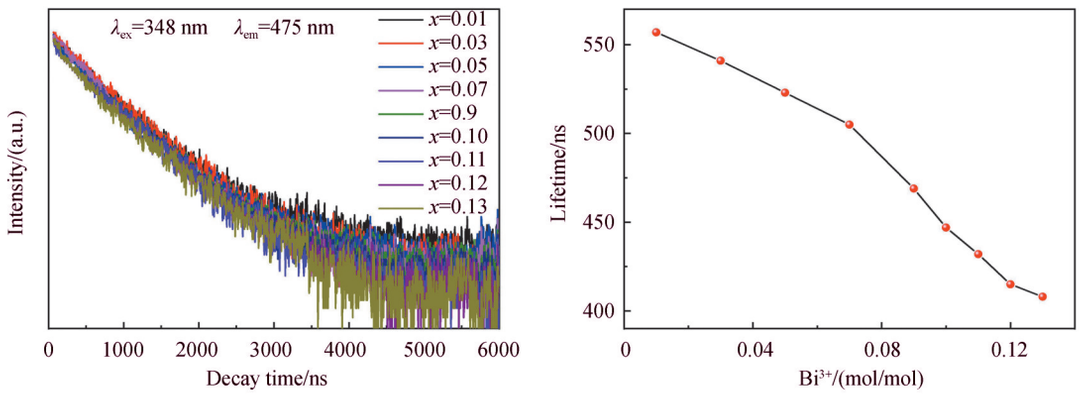

(a) Decay curves of $BaLa_{1-x}Ga_3O_7:xBi^{3+}(0.01\leqslant x\leqslant 0.13)$ samples (b) Corresponding fluorescence lifetime

图 6 $BaLa_{1-x}Ga_3O_7:xBi^{3+}(0.01\leqslant x\leqslant 0.13)$样品的衰减曲线以及对应的荧光寿命

Fig.6 Decay curves of $BaLa_{1-x}Ga_3O_7:xBi^{3+}(0.01\leqslant x\leqslant 0.13)$ samples and corresponding fluorescence lifetime

$$\eta=\frac{\int L_{\text{direct}}}{\int L_{\text{direct}}-\int L_{\text{wihtout}}} \tag{8}$$

式中，η代表量子产率，L_{direct}代表待测样品的积分强度，L_{withoutt}代表空白样品的积分强度。根据图 7 的测试数据计算分析可知，$BaLa_{0.89}Ga_3O_7:0.11Bi^{3+}$样品的$\eta$值为 19.2%，其值相对较低，因此还需进一步提高才能获得应用。

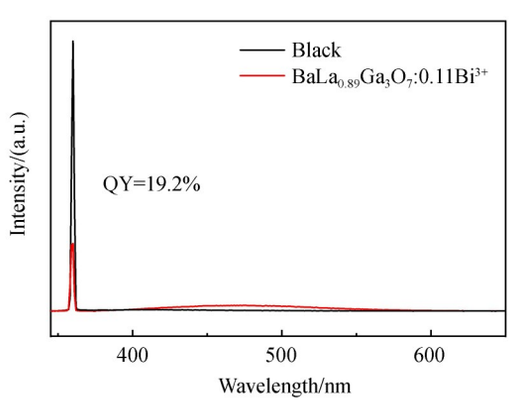

图 7 $BaLa_{0.89}Ga_3O_7:0.11Bi^{3+}$样品的量子产率

Fig.7 Quantum yield of $BaLa_{0.89}Ga_3O_7:0.11Bi^{3+}$ sample

白光 LED 长时间工作时，一部分电能会转换成热能，致使器件的内部温度升高，影响荧光粉的发光效率。因此良好的热稳定性是荧光粉实现商业化的一项基本性能要求。图 8(a)为$BaLa_{0.89}Ga_3O_7:0.11Bi^{3+}$样品在 25～200 ℃温度范围内的变温光谱。可以看出，随着温度的升高，$BaLa_{0.89}Ga_3O_7:0.11Bi^{3+}$样品的发射强度逐渐下降。如图 8(a)中的插图所示，$BaLa_{0.89}Ga_3O_7:0.11Bi^{3+}$样品在 150 ℃时的发射强度仍能保持 25 ℃时的 69.2%，说明荧光粉具有一定的热稳定性。与表 2 中列举的同类荧光粉相比，其热稳定性相对稳定。为了进一步理解这一热淬灭现象，可以通过式(9)计算样品的活化能E_a[21]。

$$\ln\left(\frac{I_0}{I}-1\right)=\ln(A)-\frac{E_a}{KT} \tag{9}$$

式中，I_0代表初始温度下的发射强度，I代表其它温度下的发射强度，A代表常数，K代表玻尔兹曼常数，T代表热力学温度。如图 8(b)所示，根据$\ln(I_0/I-1)$和$1/KT$之间的线性关系进行拟合，得到其斜率为−0.258 5，活化能E_a值可以计算出为 0.258 5 eV。

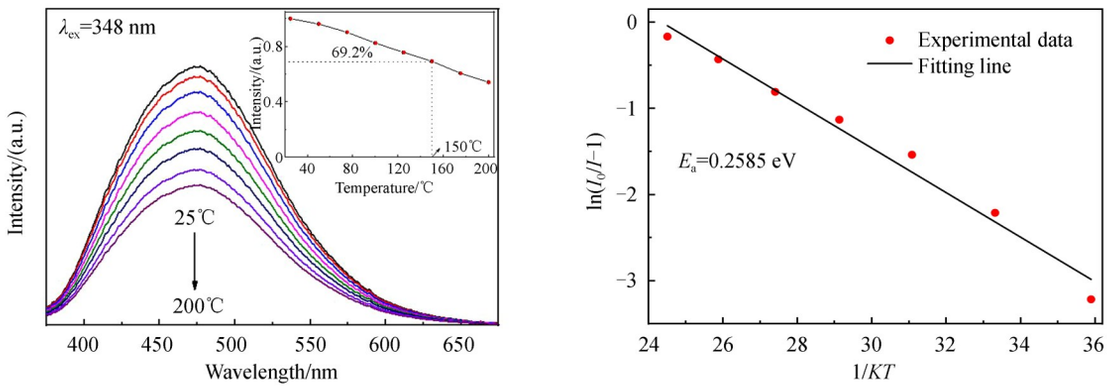

(a) Temperature-dependent PL spectra　　(b) Plot of $\ln(I/I_0-1)$ vs. $1/KT$

图 8　$BaLa_{0.89}Ga_3O_7:0.11Bi^{3+}$样品的变温光谱

Fig.8　Temperature-dependent PL spectra of $BaLa_{0.89}Ga_3O_7:0.11Bi^{3+}$ sample

表 2　Bi^{3+}掺杂荧光粉的光学性能

Table 2　Luminescence properties of some phosphors activated with Bi^{3+}

Sample	λ_{ex} /nm	λ_{em} /nm	PL Intensity at 423 K	Reference
$Cs_3Zn_6B_9O_{21}:Bi^{3+}$	322	436	100%	[6]
$NaGd_9(SiO4)_6O_2:Bi^{3+}$	340	465	76%	[7]
$Ca_3Lu_2Ge_3O_{12}:Bi^{3+}$	380	477	75%	[8]
$Ba_2Ga_2GeO_7:Bi^{3+}$	365	497	35%	[9]
$Ca_2MgWO_6:Bi^{3+}$	340	550	33%	[10]
$K_2MgGeO_4:Bi^{3+}$	335	614	85%	[22]
$BaLaGa_3O_7:Bi^{3+}$	348	475	69%	This work

4　结论

采用高温固相法合成了$BaLa_{1-x}Ga_3O_7:xBi^{3+}$ ($0.01\leqslant x\leqslant 0.13$)系列荧光粉。荧光粉样品为黄长石结构，属于四方晶系，具有P-421m空间点群结构。荧光粉颗粒呈现不规则形状，尺寸在5～30 μm之间。漫反射光谱表明$BaLaGa_3O_7$具有合适的光学带隙。$BaLa_{1-x}Ga_3O_7:xBi^{3+}$具有较宽的单一激发带和发射带，峰值分别位于348 nm和475 nm左右，归因于Bi^{3+}：$^1S_0\leftrightarrow{}^3P_1$跃迁。随着$Bi^{3+}$离子掺杂浓度的增加，样品的激发带峰值从340 nm逐渐红移到350 nm处；样品的发射带峰值位置不变，发射强度呈现先增加后减少的趋势，这一浓度猝灭现象是由偶极-偶极相互作用引起的；样品的荧光寿命呈现逐渐下降的趋势，归因于Bi^{3+}离子之间相互作用的增强。$BaLa_{0.89}Ga_3O_7:0.11Bi^{3+}$样品的发射强度最高，量子产率为19.2%；随着温度的升高，其发射强度逐渐下降，在150 ℃时的发射强度仍能保持为25 ℃时的69.2%，热淬灭的活化能为0.258 5 eV，具有一定的热稳定性。综上所述，$BaLa_{1-x}Ga_3O_7:xBi^{3+}$荧光粉在紫外激发白光LED中具有潜在的应用价值。

参考文献

[1] LIU Dongjie, YUN Xiaohan, DANG Peipei, et al. Yellow/orange-emitting $ABZn_2Ga_2O_7:Bi^{3+}$ (A=Ca, Sr; B=Ba, Sr) phosphors: optical temperature sensing and white light-emitting diode applications[J]. Chemistry of Materials, 2020, 32(7): 3065-3077.

[2] CHEN Hong, LI Chenxia, HUA Youjie, et al. Optical properties of Ce^{3+}/Eu^{2+} co-doped $Ca_3Si_2O_4N_2$ phosphors[J]. Chinese Journal of Luminescent, 2013, 34(10): 1324-1327.
陈鸿，李晨霞，华有杰，等. Ce^{3+}/Eu^{2+}共掺$Ca_3Si_2O_4N_2$荧光粉的光学特性[J]. 发光学报，2013，34(10)：1324-1327.

[3] LI Guogang, TIAN Ying, ZHAO Yun, et al. Recent progress in luminescence tuning of Ce^{3+} and Eu^{2+}-activated phosphors for pc-WLEDs[J]. Chemical Society Reviews, 2019, 44(23): 8688-8713.

[4] WANG Yuhua, DING Jianyan, WANG Yichao, et al. Structural design of new Ce^{3+}/Eu^{2+}-doped or co-doped phosphors with excellent thermal stabilities for WLEDs[J]. Journal of Materials Chemistry C, 2019, 7(7): 3480-3488.

[5] ZHENG Weixin, WU Haoyi, JU Guifang, et al. Crystal field modulation-control, bandgap engineering and shallow/deep traps tailoring-guided design of a color-tunable long-persistent phosphor (Ca, Sr)Ga_4O_7: Mn^{2+}, Bi^{3+}[J]. Dalton Transactions, 2019, 48(1): 253-265.

[6] GUAN Mengyu, WANG Wei, YAN Wei, et al. Novel narrow-band blue-emitting $Cs_3Zn_6B_9O_{21}$: Bi^{3+} phosphor with superior thermal stability[J]. Cryst Eng Comm, 2020, 22(35): 5792-5798.

[7] ZHOU Jiangcong, LAI Yiqing, WU Dewu, et al. Site-selective excitation and photoluminescence properties of a cyan-emitting $NaGd_9(SiO_4)_6O_2$: Bi^{3+}phosphor for potential application in white light-emitting diodes[J]. Ceramics International, 2021, 47(10): 133769-13775.

[8] YE Shanshan, LIU Hai, WANG Yijie, et al. Design of a bismuth-activated narrow-band cyan phosphor for use in white light emitting diodes and field emission displays[J]. ACS Sustainable Chemistry & Engineering, 2020, 8(49): 18187-18195.

[9] LI Huimin, PANG Ran, LUO Yangqing, et al. Structural micromodulation on Bi^{3+}-doped $Ba_2Ga_2GeO_7$ phosphor with considerable tunability of the defect-oriented optical properties[J]. ACS Applied Electronic Materials, 2019, 1(2): 229-237.

[10] CAO Renping, QUAN Guanjun, SHI Zhihui, et al. A double perovskite Ca_2MgWO_6: Bi^{3+} yellow-emitting phosphor: synthesis and luminescence properties[J]. Journal of Luminescence, 2017, 181: 332-336.

[11] HU Songhan, LONG Zhangwen, WEN Yugeng, et al. An orange-emitting phosphor $BaSrGa_4O_8$: Bi^{3+}, K^+ with unique one-dimensional chain structure for high index color WLEDs[J]. Journal of the American Ceramic Society, 2020, 103(11): 6075-6080.

[12] GAO Shufang, XU Shan, WANG Yeqing, et al. Spectral characteristics and white emission of Dy^{3+}/Tm^{3+}-$BaLaGa_3O_7$ phosphors[J]. Journal of Luminescence, 2016, 178: 282-287.

[13] GAO Shufang, ZHENG Kexin, XU Shan. Luminescence properties and energy transfer behavior of $BaLaGa_3O_7$: Pr^{3+}, Tb^{3+} phosphors for ultraviolet excited white light-emitting diodes[J]. Materials Express, 2018, 8(4): 368-374.

[14] LV Wenzhen, LU Wei, GUO Ning, et al. Efficient sensitization of Mn^{2+} emission by Eu^{2+} in $Ca_{12}Al_{14}O_{33}Cl_2$ host under UV excitation[J]. RSC Advances, 2013, 3(36): 16034-16039.

[15] OHKO Y, HASHIMOTO K, FUJISHIMA A. Kinetics of photocatalytic reactions under extremely low-intensity UV illumination on titanium dioxide thin films[J]. Journal of Physical Chemistry A, 1997, 101(43): 8057-8062.

[16] WANG Yao, GUO Ning, SHAO Baiqi, et al. Adjustable photoluminescence of Bi^{3+} and Eu^{3+} in solid solution constructed by isostructural end components through composition and excitation-driven strategy[J]. Chemical Engineering Journal, 2021, 421: 127735.

[17] BLASSE G. Energy transfer in oxidic phosphors[J]. Physical Letters, 1968, 28(6): 444-445.

[18] LIU Feng, LIANG Yanjie, CHEN Yafei, et al. Divalent nickel-activated gallate-based persistent phosphors in the short-wave infrared[J]. Advanced Optical Materials, 2016, 4(4): 562-566.

[19] ZHANG Xinmin, SEO H J. Color tunable and thermally stable luminescence of Tb^{3+} doped $Li_4SrCa(SiO_4)_2$phosphors[J]. Materials Research Bulletin, 2012, 47(8): 2012-2015.

[20] LIU Quan, XIONG Puxian, LIU Xiaoqi, et al. Deep red $SrLaGa_3O_7$: Mn^{4+} for near ultraviolet excitation of white light LEDs[J]. Journal of Materials Chemistry C, 2021, 9(11): 3969-3977.

[21] XIAO Jianhua, CAO Jiangkun, WANG Yafei, et al. Temperature dependent energy transfer in Bi/Er codoped barium gallogermanate glasses for tunable and broadband NIR emission[J]. Journal of Materials Chemistry C, 2019, 7(34): 10544-10550.

[22] LI Huimin, PANG Ran, LIU Guanyu, et al. Synthesis and luminescence properties of Bi^{3+}-activated K_2MgGeO_4: a promising high-brightness orange-emitting phosphor for WLEDs conversion[J]. Inorganic Chemistry, 2018, 57(19): 12303-12311.

Synthesis and Luminescent Properties of $BaLaGa_3O_7$: Bi^{3+} Phosphors

LIANG Dongbao, ZHANG Rui, SHEN Yufang, ZHANG Jian

(*Key Laboratory of Nonferrous Materials and New Processing Technology, Ministry of Education, Guangxi Key Laboratory of Optical and Electronic Materials and Devices, College of Materials Science and Engineering, Guilin University of Technology, Guilin, Guangxi* 541004, *China*)

Abstract: At present, with the increasingly serious environment and energy, the research and development of green and low energy consumption technology has attracted extensive attention. In the field of lighting, as a green light source in the 21st century, phosphor-converted White Light-Emitting Diodes (WLEDs) are expected to become an indispensable generation of comfortable and healthy lighting system due to its

obvious advantages of high luminous efficiency, low environmental pollution and low energy consumption. The two key materials for commercially available WLEDs are yellow YAG:Ce phosphors and blue LED chips. In this scheme, the lack of red component results in only a low color rendering index (<80), high related color temperature (>4 500 K) cold white light, which are not conducive to the application of indoor lighting. Generally speaking, adding efficient red phosphors on this basis can obtain a higher color rendering index and a lower color temperature. However, one of the costs of adding such phosphors is that the device becomes significantly less efficient. From a more comprehensive and humanized perspective, the combination of ultraviolet LED chip with red, blue and green phosphors has undoubtedly attracted the attention of the majority of scientific researchers. As far as we know, rare earth ions (such as Eu^{2+} and Ce^{3+}) are used as activators for most of the phosphors that can be excited by ultraviolet LED chips and tricolor phosphors in the lighting scheme. However, the mixture of three primary phosphors can easily cause spectral reabsorption. In addition, an imbalance between supply and demand makes rare earths expensive, which is a major impediment to their commercialization. In view of this situation, choosing phosphors with non-rare earth ions as activators can effectively solve the above problems of rare earth doped phosphors. Nowadays, as another type of activator, bismuth (Bi), has been extensively studied and reported because of the potential optical properties related to the strong interaction with surrounding coordination environments and abundant valence states. In this paper, a series of $BaLa_{1-x}Ga_3O_7:xBi^{3+}$ ($0.01 \leqslant x \leqslant 0.13$) phosphors were synthesized through traditionnal high temperature solid state method. The X-ray diffraction patterns and rietveld refinement results indicate the pyrite structure of above samples. Scanning electron microscope images show that the phosphor particles are irregular in shape with the size of 5～30 μm. Diffuse reflectance spectra of $BaLaGa_3O_7$ matrix indicate a suitable optical band gap for Bi^{3+} luminescence. When Bi^{3+} substitutes La^{3+}, the excitation wavelength has a red shift from 340 to 350 nm. Under the excitation of 348 nm ultraviolet light, $BaLa_{1-x}Ga_3O_7:xBi^{3+}$ phosphors exhibit one evident emission peak at 475 nm. With the increase of Bi^{3+} concentration, the emission intensity firstly increased and then decreased, and this optical phenomenon is generally considered to be related to the concentration quenching. Among them, the emission intensity of $BaLa_{0.89}Ga_3O_7:0.11Bi^{3+}$ phosphor reaches the maximum with a quantum yield of 19.2%, and the emission intensity at 150 ℃ still maintains 69.2% of that at 25 ℃. It indicates that the $BaLa_{1-x}Ga_3O_7:xBi^{3+}$ phosphors have potential application value in the field of near ultraviolet excitied white LEDs.

Key words: Bi^{3+} ion; Gallate; Phosphors; Photoluminescence properties; White LEDs

OCIS Codes: 160.2100; 160.2540; 160.4670

Foundation item: National Natural Science Foundation of China (No. 52062008), Guangxi Natural Science Foundation (No.2018GXNSFAA050021)